

## **DYNAMIC FRACTURE OF CONCRETE IN COMPRESSION: 3D FINITE ELEMENT ANALYSIS AT MESO- AND MACRO-SCALE**

## **DYNAMISCHER BRUCH VON BETON UNTER DRUCK: 3D-FINITE-ELEMENT-ANALYSE AUF MESO- UND MAKRO-SKALA**

Serena Gambarelli<sup>1</sup>, Joško Ožbolt<sup>2</sup>

<sup>1</sup> *Materials Testing Institute (MPA), University of Stuttgart, Otto-Graf-Institute*

<sup>2</sup> *Institute of Construction Materials, University of Stuttgart*

### **SUMMARY**

In the present paper the fracture of normal strength concrete cylinder under static and dynamic compressive loading is numerically investigated. 3D finite element simulations are carried out at macro- and meso-scale. The coarse aggregate is assumed to be linear elastic and mortar is modelled using rate-dependent microplane model. The comparison between meso-scale and macro-scale analysis shows that the macroscopic analysis is principally able to account for the major effects related to dynamic fracture of concrete. Dynamic resistance of concrete in compression (apparent strength) depends on a number of parameters and it is mainly influenced by the inertia effects that are closely related to the load induced damage [1].

### **ZUSAMMENFASSUNG**

In der vorliegenden Arbeit wird das Versagen von Zylindern aus normalfestem Beton unter statischer und dynamischer Druckbelastung numerisch untersucht. 3D-Finite-Elemente-Simulationen auf Makro- und Meso-Skala wurden durchgeführt. Der Zuschlag ist als linear elastisch angenommen und Mörtel ist mit dem dehngeschwindigkeitsabhängigen Mikroplane Modell modelliert. Der Vergleich zwischen der Analyse auf Meso- und Makro-Skala zeigt, dass die makroskopische Analyse prinzipiell in der Lage ist, die wichtigsten Effekte, die im Zusammenhang mit dem dynamischen Betonversagen sind, realistisch zu berücksichtigen. Die dynamische Betondruckfestigkeit (scheinbare Festigkeit) hängt von einer Reihe von Parametern ab und ist hauptsächlich von den Trägheitseffekten beeinflusst, die in engem Zusammenhang mit der belastungsinduzierten Schädigung des Betons stehen [1].

## 1. INTRODUCTION

Understanding dynamic fracture behavior of concrete at high strain rates is fundamental for the safety assessment and design of concrete structures subjected to dynamic loading (impact and blast). It is well known that the behavior of concrete structures is strongly influenced by the loading rate [2]. Compared to quasi-static loading, concrete under impact load acts in a different way. First, there is a strain-rate influence on strength, stiffness, and ductility, and, second, there is inertia activated which influence the resistance and failure mode of concrete. The results of dynamic experimental tests show that after reaching some critical strain rate concrete resistance progressively increases with increase of strain rate. This type of the response is typical for many different problems, e.g. compression, direct tension, bending, pull-out of anchors, etc. [2, 3].

The compressive strength of concrete under dynamic loading is usually tested using hydraulic machines, drop hammer machines and split Hopkinson pressure bars (SHPB). Based on the available test results, the compressive dynamic increase factor (CDIF), defined as the ratio of dynamic and static resistance, has been introduced to derive some empirical formulae evaluating the strength enhancement as a result of the strain rate effect [4-6].

Although the definition of dynamic compressive strength through the CDIF factor has attracted considerable interest in structural design, it should be pointed out that the strength enhancement of concrete at high loading rates is not a material property. As shown in [7], a relevant scatter of the CDIF data has been detected in all available experimental tests. The reasons for the contrasting results have been widely discussed, with the conclusion that the strength enhancement of concrete under dynamic compressive loading is influenced by several parameters, partially related to the material itself and partially to the structural effects. For relatively low loading rates the moderate increase of resistance with increasing loading rate is mainly controlled by the strain rate dependent response of concrete. This is partly due to the inertia at material micro-scale and partly is a consequence of the viscous response of concrete due to the water content. These two effects can be accounted for by the constitutive law. However, the main reason for the progressive increase of resistance with increase of loading rate is activation of inertia at the macro-scale that is due to different reasons such as: structural inertia, inertia due to hardening or softening of concrete, crack propagation and crack branching [1, 2, 8]. When modeling at meso- or macro-scale these effects should

be automatically accounted for [2] whereas the rate effect coming from the material micro level have to be covered by the constitutive law. It is important to note that principally the rate sensitive constitutive law should not directly be compared with the results of dynamic test. Namely, to filter out different effects of inertia the test results must be compared with the results of simulations, i.e. the objective rate sensitive constitutive law can be obtained only by fitting the test results with the results of numerical simulation.

A limited number of studies can be found in the literature dealing with 3D meso-scale modeling of concrete under dynamic compressive loading [9-10]. Thus, in the present paper, the dynamic compressive behavior of normal strength concrete, with strain rate up to  $200 \text{ s}^{-1}$ , is numerically investigated through 3D macro- and meso-scale analysis of a concrete cylinder ( $L/D = 2$ ). The paper is organized as follows. Section 2 describes the procedure to generate the meso-scale model, the computational background and the material parameters. In section 3 the obtained results, in terms of stress-strain curves (both load and reaction) and crack patterns, are presented for static and dynamic loading at different strain rates. The main conclusions are given in section 4.

## 2. GENERATION OF 3D MESO-SCALE FINITE ELEMENT MODEL

### 2.1 RANDOM AGGREGATE STRUCTURE IN CONCRETE

To generate meso-scale structure of concrete, the coarse aggregate with a specific size distribution, is randomly distributed inside the concrete cylinder by using a simple generation procedure implemented in Matlab R2013b. The procedure is based on two distance criteria: the first one prevents any contact between the generated particles and the external boundaries of the cylinder and the second one avoids the intersection between adjacent particles (assumed spherical). The size distribution of the coarse aggregate is determined by using the Fuller curve (Eq. 1):

$$p(d) = 100 \left( \frac{d}{d_{max}} \right)^q \quad (1)$$

where  $p(d)$  is the corresponding passing amount (%),  $d$  is the diameter of each granulometric class,  $d_{max}$  is the maximum aggregate diameter and  $q$  is the exponent of the chosen granulometric curve. The number of particles of each granulometric class is determined as follows: (1) Based on the given values of  $d_{max}$

and  $q$ , the passing amount  $p(d)$  is evaluated using Eq. 1; (2) The retained amount (%) is then calculated as the difference between the adjacent classes' passing; (3) Knowing the retained percent of every class, the total volume of the class and the corresponding number of aggregates are evaluated and (4) Spherical particles are randomly placed in the domain, guaranteeing no intersection between any of them. Based on three different granulometric classes ( $d = 5, 7.5, 10$  mm), spheres are inserted from largest to smallest (see Fig. 1).

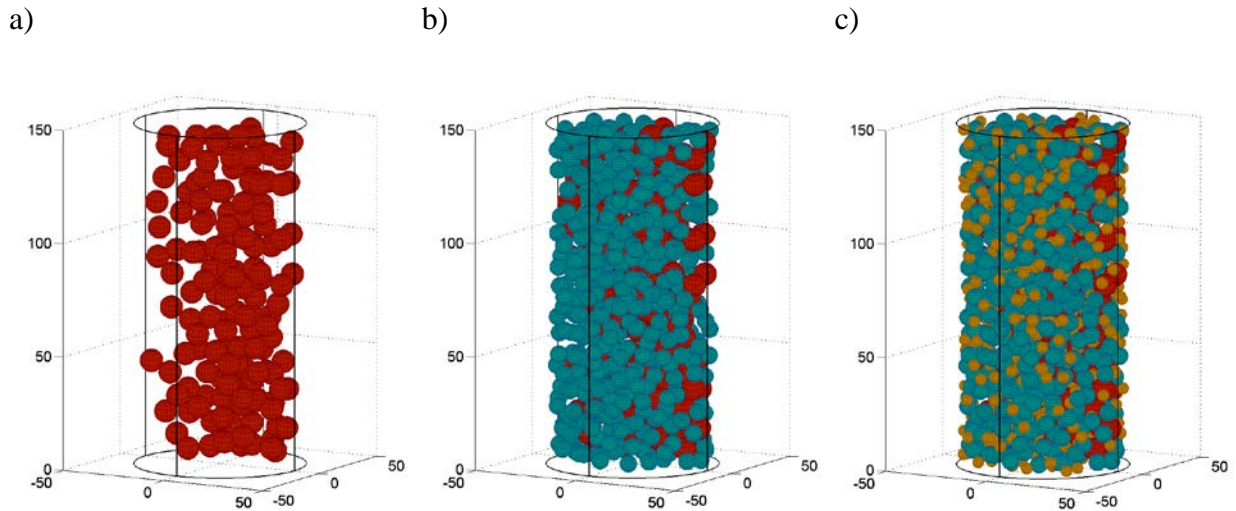


*Fig. 1: Insertion of particles in the cylinder (three different granulometric sizes)*

A volume fraction of 28% of the coarse aggregate ( $5 \text{ mm} \leq d \leq 10 \text{ mm}$ ) is reproduced in the model. The geometry of the created meso-models was imported into the 3D FE code MASA used for the simulations and meshed with approximately  $10^6$  solid four-node constant strain finite elements. The same as for the mortar, macro-scale finite element discretization was performed using constant strain four-node solid finite elements.

## 2.2 MATERIAL PROPERTIES

In the 3D meso-scale FE analysis the constitutive law for mortar is based on the rate-dependent microplane model proposed by Ožbolt et al. [11], while the aggregate is considered as linear elastic with Young's modulus of 60 GPa and Poisson's number 0.18 (limestone). The ratio of the elastic moduli of the aggregate and matrix phase is set at 3:1, with  $E = 20$  GPa. The material properties used for the macro and meso-scale analysis are summarized in Table 1. It is worth men-

tioning that in both modeling approaches the model parameters have been calibrated to correctly reproduce the uniaxial compressive behavior of normal strength concrete (see section 3).

Table 1: Material properties (macro- vs. meso-model)

Mechanical properties	Macro-model	Meso-model	
	Concrete	Aggregate	Mortar
Initial elastic modulus, $E$ [GPa]	37.0	60.0	20.0
Poisson' ratio, $\nu$	0.18	0.18	0.18
Compressive strength, $f_c$ [MPa]	23.0	-	26.0
Tensile strength, $f_t$ [MPa]	2.3	-	2.6
Fracture energy, $G_F$ [J/m <sup>2</sup> ]	60	-	20
Mass density, $\rho$ [kg/ m <sup>3</sup> ]	2300	2700	2100

### 2.3 RATE-DEPENDENT MICROPLANE MODEL AND 3D FE ANALYSIS

In the numerical simulations the rate sensitive microplane model [11] is employed as constitutive law. In the model the influence of strain rate is accounted for through two effects: (1) The rate dependency due to viscosity of the bulk material and (2) The rate dependent growth of micro-cracks. The influence of structural inertia effects on the rate dependency is not a part of the constitutive law, however, it is automatically accounted for in the dynamic analysis. In the microplane model macroscopic response is obtained by integrating normal and shear microplane stresses overall microplanes. The rate independent microplane stress components  $\sigma_{Mp}^0(\varepsilon_{Mp})$  ( $Mp$  stands for microplane volumetric, deviatoric and shear components, respectively) are calculated from the known microplane strains  $\varepsilon_{Mp}$  using pre-defined microplane uniaxial stress-strain constitutive relations [12]. The strain rate independent model parameters are: Young's modulus, Poisson's ratio, uniaxial compressive and tensile strengths and fracture energy. The rate effect on each microplane component is of the same type as proposed by Bažant et al. [13, 14]:

$$\sigma_{Mp}(\varepsilon_{Mp}) = \sigma_{Mp}^0(\varepsilon_{Mp}) \left[ 1 + c_2 \ln \left( \frac{2\dot{\gamma}}{c_1} \right) \right] ; \text{ with } \dot{\gamma} = \sqrt{\frac{1}{2} \dot{\varepsilon}_{ij} \dot{\varepsilon}_{ij}} \quad c_1 = \frac{c_0}{s_{cr}} \quad (2)$$

where  $c_1$  and  $c_2$  are material rate constants, which were calibrated by fitting the uniaxial compressive tests performed by Dilger et al. [15], and  $\dot{\varepsilon}_{ij}$  is the macroscopic strain rate tensor. Note that the strain rate is not measured on the individual

microplanes, but on the macro-scale. In the present computations  $c_1 = 4.0 \times 10^{-6} \text{ s}^{-1}$  and  $c_2 = 0.032$ . Furthermore, Eq. 2 applies to all microplane components except to volumetric compression, which is assumed to be rate insensitive. It has to be noted that the material rate constants in Eq. 2, calibrated for concrete, are also used for mortar at the meso-scale analysis. In Table 2 is given a summary of rate dependent mechanical properties of concrete (macro analysis) and mortar (meso-analysis).

Table 2: Rate dependent fracture properties (constitutive law, Eq. 2) of concrete and mortar

Material	Property	Static	50 s <sup>-1</sup>	100 s <sup>-1</sup>	150 s <sup>-1</sup>	200 s <sup>-1</sup>
Concrete	$f_c$ [MPa]	23.3	38.9	39.5	39.8	40.0
	$f_t$ [MPa]	2.3	3.62	3.67	3.70	3.72
	$G_F$ [J/m <sup>2</sup> ]	60.0	108.0	109.8	110.4	111.0
Mortar	$f_c$ [MPa]	26.0	43.3	43.8	44.2	44.5
	$f_t$ [MPa]	2.6	4.20	4.26	4.30	4.32
	$G_F$ [J/m <sup>2</sup> ]	20.0	42.8	43.4	43.6	44.0

### 3. INFLUENCE OF STRAIN RATE ON THE CONCRETE COMPRESSIVE FAILURE: MESO- VS. MACRO-ANALYSIS

The influence of the strain rate on dynamic compressive behavior of concrete is investigated by means of meso- and macro-scale modeling approaches. 3D FE analysis of concrete cylinder ( $L/D = 150/75 \text{ mm}$ ) at different average strain rates ( $50 - 200 \text{ s}^{-1}$ ) was carried out. Static analysis (no rate effect) was also performed.

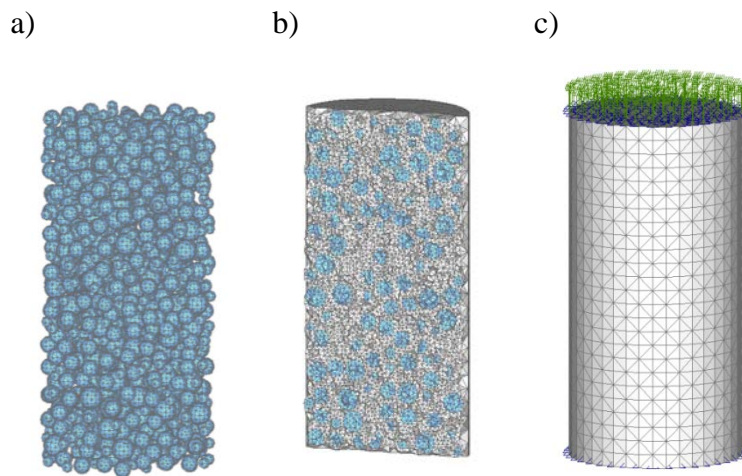


Fig. 2: 3D FE meso-scale model: a) coarse aggregate; b) meso-scale material structure (internal section) and c) FE model with vertical displacement and boundary conditions

Upper and lower loading surfaces of the cylinder were fully restrained in the loading plane. The load was applied by controlling displacement  $\delta$  of the upper surface of the cylinder in the vertical direction (Fig. 2).

### 3.1 STATIC ANALYSIS

The numerical results, in terms of axial stress-strain curves and concrete failure mode, obtained from the static analysis are shown in Figs. 3 and 4, respectively. It can be seen that both the macro and meso-models are able to correctly reproduce the typical compressive curve of normal strength concrete ( $f_c = 23.5$  MPa,  $\varepsilon_{peak} = 0.0025$ ,  $E = 27$  GPa) for pre- and post-peak responses (Fig. 3). Note that the internal microplane model parameters were chosen such that static meso- and macro-scale 3D FE analyses give approximately the same response.

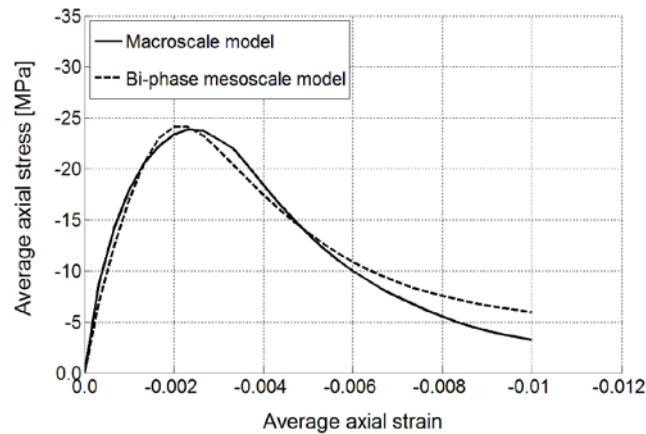


Fig. 3: Static uniaxial compressive test: average stress-strain curve

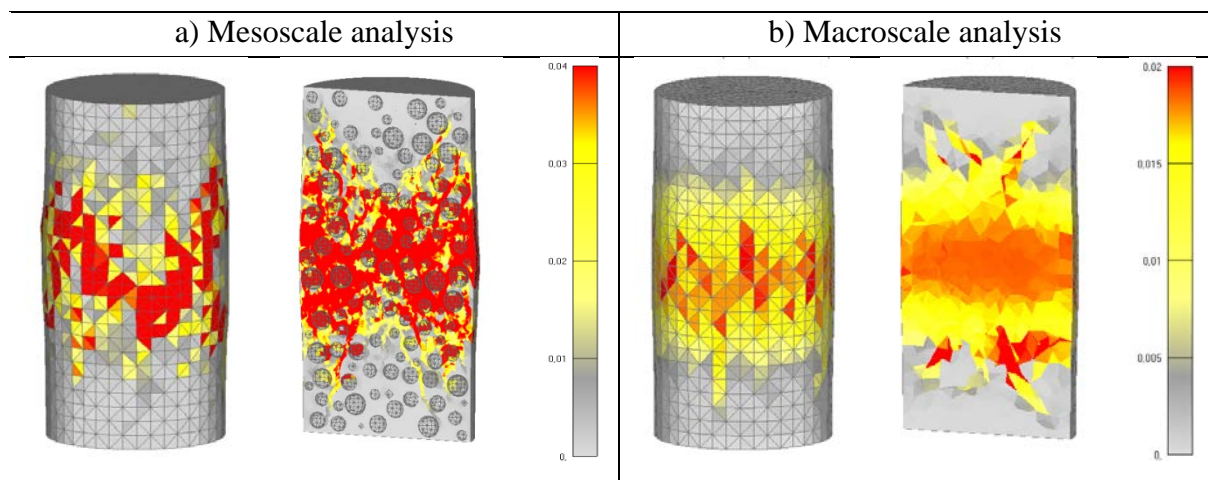


Fig. 4: Typical failure mode obtained in the static FE analysis: a) meso-scale and b) macro-scale

The typical failure mode obtained in the static analysis is shown in Fig. 4. Damage in mortar and concrete is represented in terms of maximum principal strains, where the dark zones correspond to the crack width of 0.15 mm or greater. Due to the fixed boundary conditions, diagonal shear failure takes place at the mid of the cylinder height. To show the internal damage distribution the specimen has been cut at mid-section. Similarly as in the experiments, the typical hourglass shape of concrete at the final stage of the loading history is observed.

### 3.2 DYNAMIC ANALYSIS

The direct integration scheme of explicit type was employed in the dynamic analysis, with damping set to 1000 [N s/mm]. This value was used based on the calibration of the numerical model [2, 3]. The analysis was performed for high strain rates ( $50 \div 200 \text{ s}^{-1}$ ). The summary of the calculated compressive resistances (loads and reactions) is reported in Table 2. Due to the high loading rates the compressive resistances at loaded top of the cylinder (apparent strength) from the dynamic analysis are significantly higher than the static strength of concrete. However, it can be also seen that the resistance on the reaction (bottom) side of the specimen is only slightly higher than the static strength of the specimen and, as will be shown below, it approximately follows the rate dependent constitutive law. The loading stress, which is in equilibrium with structural inertia that is generated as a consequence of concrete damage, is much higher than the reaction stress. The effect is the same as discussed in [3] for the case of uniaxial tension.

Table 2: Dynamic analysis – summary of the calculated apparent strength [MPa]

FE Analysis		Static	50 s <sup>-1</sup>	100 s <sup>-1</sup>	150 s <sup>-1</sup>	200 s <sup>-1</sup>
Macro-scale	Load	23.3	66.8	120.9	170.4	218.5
	Reaction	23.3	45.2	39.4	42.2	67.6
Meso-scale	Load	23.8	56.2	100.3	137.1	173.1
	Reaction	23.8	46.8	54.9	58.1	60.0

From Table 2 can also be seen that the resistance at the loaded side of the cylinder is consistently higher in case of macro-scale analysis than in the meso-scale analysis. The reason is due to the fact that the aggregate is linear elastic, i.e. in the aggregate no inertia and rate sensitivity due to damage is generated.

In Fig. 5 the loading and reaction stresses, obtained by dividing respectively the global axial force and reaction over the concrete section area, are plotted against time. The results from the macro analysis (black curves) are compared with those obtained at meso-scale (grey curves). In both cases there is a progressive increase of the loading compressive stress with the increase of loading rate. However, as mentioned above, the reaction stresses are increasing only slightly with the loading rate.

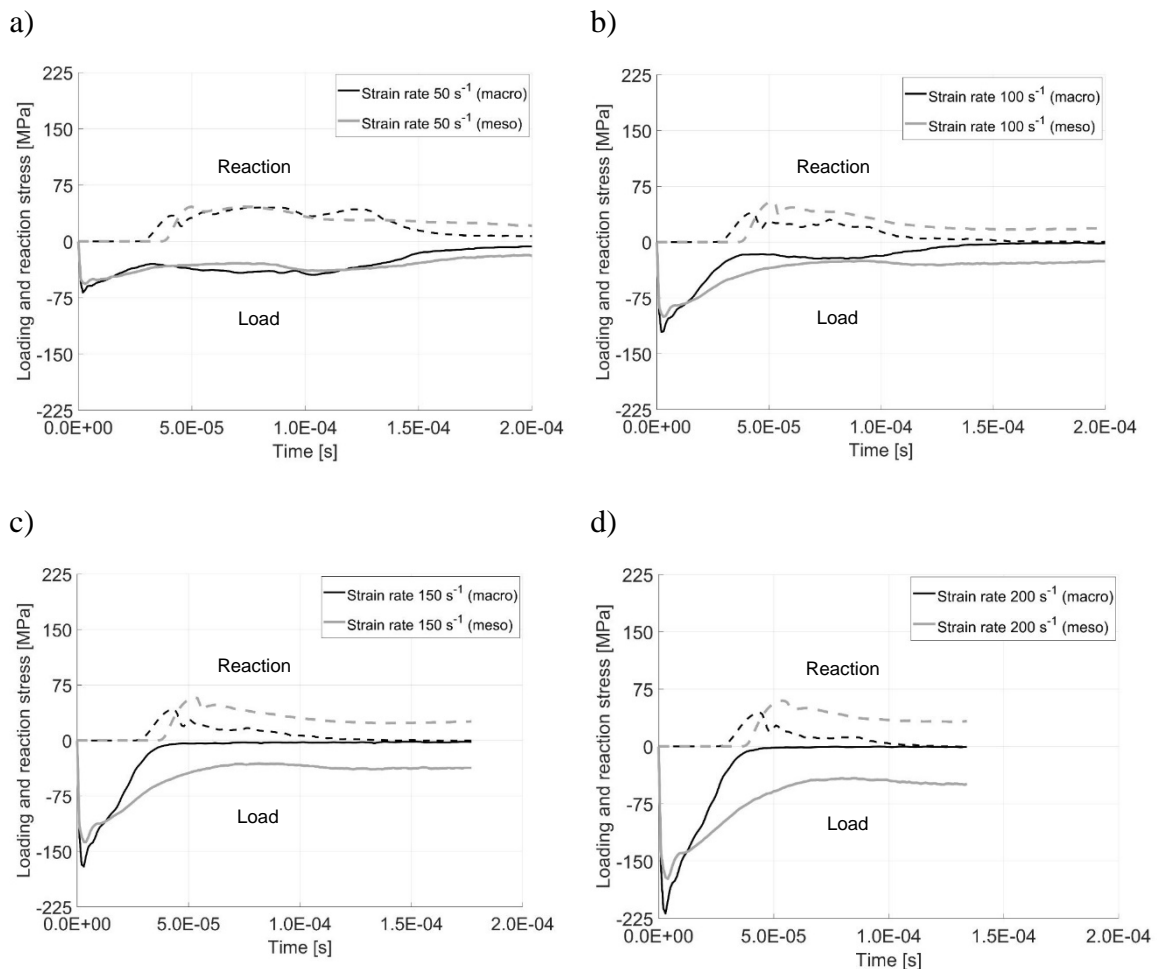


Fig. 5: Calculated stress-time curves at different loading rates: a) 50 s<sup>-1</sup>; b) 100 s<sup>-1</sup>; c) 150 s<sup>-1</sup> and d) 200 s<sup>-1</sup>

Furthermore, it can be seen (Fig. 5) that the reaction stress is even not activated at the time when the loading stress reaches its maximum. With decrease of the loading rate the observed delay and the difference between the reaction and loading stresses is decreasing, i.e. with the strain rate approaching to zero (quasi-static loading) there is no delay and both stresses are the same. However, in terms of

time the activation of reaction stress is approximately the same in all cases and it is in the range of  $3.2 \times 10^{-5}$  s.

In case of meso-scale analysis (red curves in Fig. 5), appreciable residual stresses are observed at the end part of the stress-time curve. To prove that the residual stress is caused by the linear elastic behavior of grains, a meso-scale dynamic analysis for the strain rate  $200 \text{ s}^{-1}$  was carried out assuming non-linear behavior of the coarse aggregate. The assumed aggregate mechanical properties are reported in Fig. 6a and the obtained stress-time curves are shown in Fig. 6b. All other properties are the same as specified Table 1. It is seen (see Fig. 6b) that the dynamic response of concrete is not significantly affected by the aggregate non-linearity. However, since the aggregate can also get damaged the axial stress reduces approximately to zero.

a)

Mechanical properties	Aggregate
Initial elastic modulus, $E$ [GPa]	90
Poisson' ratio, $\nu$	0.18
Compressive strength, $f_c$ [MPa]	100
Tensile strength, $f_t$ [MPa]	10
Fracture energy, $G_F$ [J/m <sup>2</sup> ]	40
Mass density, $\rho$ [kg/ m <sup>3</sup> ]	2700

b)

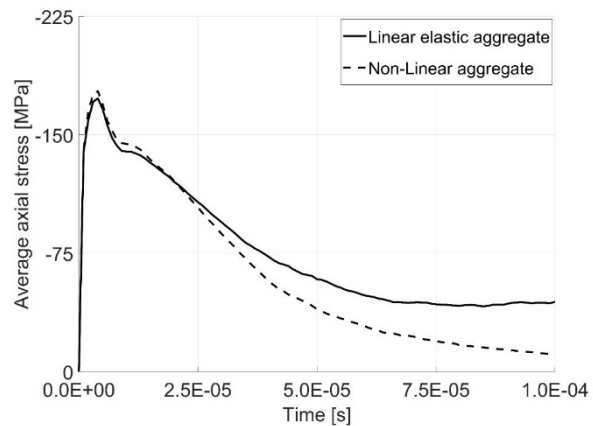


Fig. 6: a) Mechanical properties of coarse aggregate; b) Stress-strain curves at strain rate  $200 \text{ s}^{-1}$  (loaded surface)

The evolution of damage in mortar (meso-scale) and concrete (macro-scale), for the strain rates  $50$  and  $200 \text{ s}^{-1}$  is shown in Figs. 7 and 8. Concerning the case with strain rate of  $50 \text{ s}^{-1}$  (Fig. 7), the damage is mainly localized in the middle part of the specimen and similar results are obtained for both models, i.e. macro and meso. At the end of the loading process, the typical hourglass shape of the specimen, as in the static simulation, can be observed (Fig. 7a). For very high strain rate (Fig. 8) damage localization takes place in the upper part of the specimen, close to the loading surface. Due to end friction confinement, failure of the specimen occurs slightly away from the loading surface. The results obtained for

macro-scale analysis are similar to that achieved at meso-scale, confirming the predictability of both models.

According to CEB recommendation, the dependence of CDIF on strain-rate reads:

$$CDIF = \frac{f_{cd}}{f_{cs}} = \left[ \frac{\dot{\varepsilon}}{\dot{\varepsilon}_s} \right]^{1.026\alpha_s} \quad \text{for } \dot{\varepsilon} \leq 30 \text{ s}^{-1} \quad (3a)$$

$$CDIF = \gamma_s \left[ \frac{\dot{\varepsilon}}{\dot{\varepsilon}_s} \right]^{\frac{1}{3}} \quad \text{for } \dot{\varepsilon} > 30 \text{ s}^{-1} \quad (3b)$$

where  $f_{cs}$  and  $f_{cd}$  are the unconfined uniaxial compressive strengths from the static and dynamic tests,  $\gamma_s = 10^{(6.156\alpha_s - 2.0)}$ ,  $\alpha_s = 1/(5 + 9 f_{cs}/f_{c0})$ ,  $\dot{\varepsilon}_s = 30 \times 10^{-6}$  and  $f_{c0} = 10$  MPa.

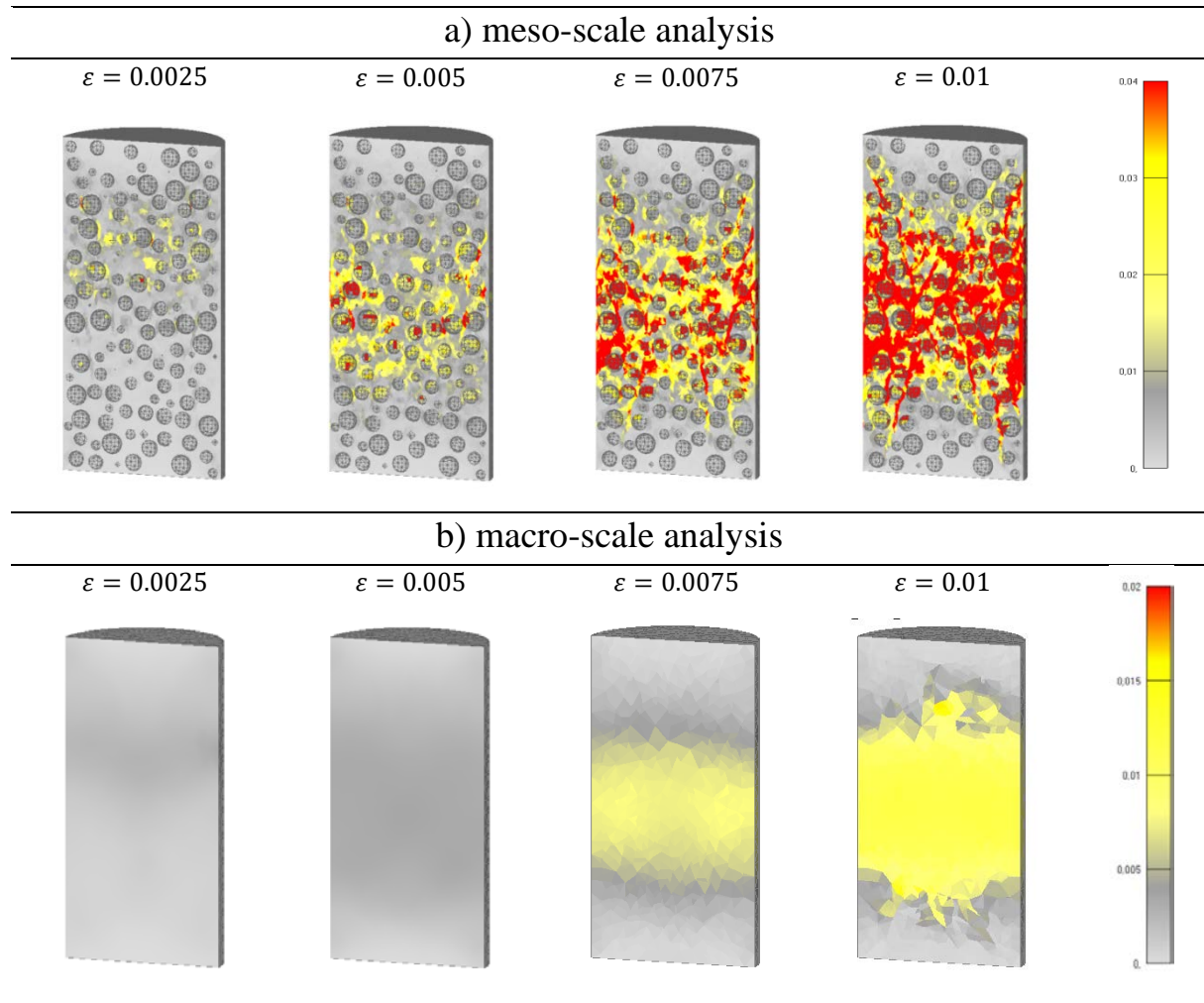


*Fig. 7: Evolution of damage under strain rate  $50 \text{ s}^{-1}$ : a) meso-scale analysis; b) macro-scale analysis*

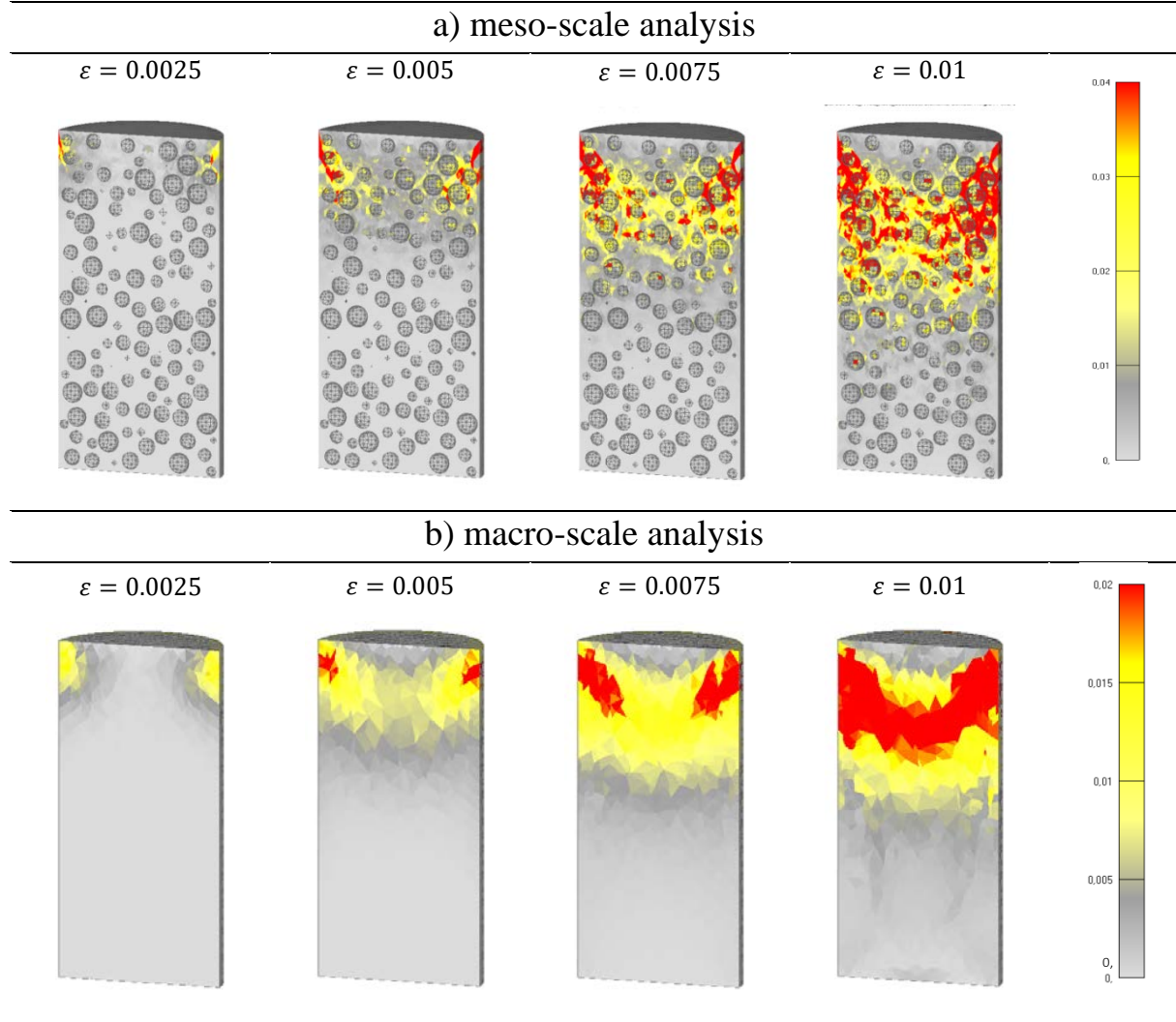


Fig. 8: Evolution of damage under strain rate  $200 \text{ s}^{-1}$ : a) meso-scale analysis; b) macro-scale analysis

The strain-rate effect on CDIF of concrete obtained by means of macro- and meso-scale FE analysis and according to the CEB prediction formula (Eq. 3) are shown in Fig. 9. Both, the CDIF values measured at the top and at the bottom surfaces of the specimen (loading and reaction stresses) are shown and also compared with the used rate-sensitive constitutive law. The first observation is that in both approaches the inertia activated in the damage zone of the specimen mainly controls the progressive increase of the peak loading stresses (apparent strength). However, inertia has not strong influence on the peak reaction stresses. The peak reaction stress exhibits a trend that is close to that of the strain rate sensitive constitutive law, with almost no influence of structural inertia effects.

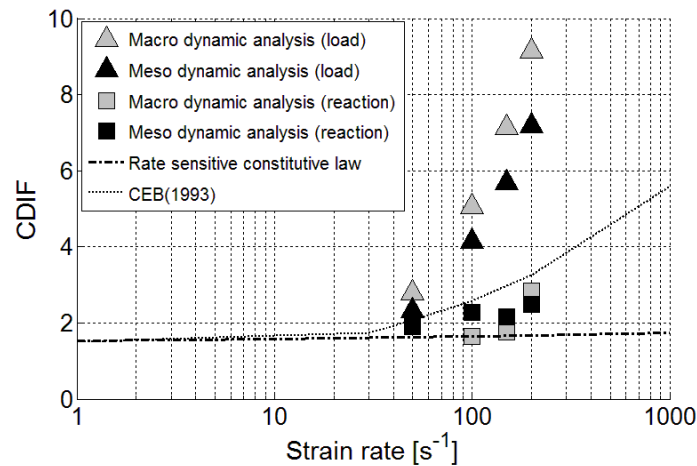


Fig. 9: CDIF curves: numerical results, CEB formula and rate-sensitive constitutive law

Since the inertia effects predominantly influence dynamic compressive resistance it is clear that such compressive resistance depends not only on the material properties but also on the geometry and size of the specimen, frictional effects on the loading surfaces, test setup, etc. [1]. Consequently, the measured resistance for relatively high loading rates is not the dynamic strength of concrete and CDIF is not representing the true material strength.

#### 4. CONCLUSIONS

In the present paper failure of normal strength concrete cylinder under static and dynamic compressive loading is studied numerically. 3D finite element analysis was performed at meso- and macro-scale. Based on the results of the simulations the following can be concluded. (i) It is shown that compressive resistance of concrete at high strain rate progressively increases with the strain rate. However, this is the case only for the loading part of the cylinder. In contrary to this, the resistance on the reaction side of the specimen approximately follows the rate sensitive constitutive law. The main reason for progressive increase of resistance is damage induced inertia which is automatically accounted for in dynamic finite element analysis. The results are in good agreement with experimental observations; (ii) It is demonstrated that macro-scale approach is able to correctly predict dynamic compressive fracture of concrete. The failure mode in meso- and macro-scale analysis is principally the same, however, the resistance of the macro model is slightly higher. The reason is due to the fact that in the meso scale analysis the aggregate exhibits no damage and no rate sensitivity (linear elastic); (iii) Because dynamic resistance of concrete for relatively high loading rates depends on inertia,

compressive dynamic increase factor (CDIF), such as defined in current design codes, does not represent rate dependent compressive strength of concrete.

## REFERENCES

- [1] GAMBARELLI, S., OŽBOLT, J.: *Dynamic Fracture of Concrete in Compression: 3D Finite Element Analysis at Meso- and Macro-scale*, Continuum Mech. Thermodyn., <https://doi.org/10.1007/s00161-020-00881-5>
- [2] OŽBOLT, J., BOŠNIAK, J., SOLA, E.: *Dynamic fracture of concrete compact tension specimen: experimental and numerical study*, Int. J. Solids Struct., 50, 4270-4278 (2013)
- [3] OŽBOLT, J., SHARMA, A., IRHAN, B., SOLA, E.: *Tensile behavior of concrete under high loading rates*, Int. J. Impact. Eng., 69:55-68 (2014)
- [4] TEDESCO, J.W., ROSS, CA.: *Strain-rate-dependent constitutive equations for concrete*, ASME J. Press. Vessel Technol., 120:398-405 (1998)
- [5] GROTE, D.L., PARK, S.W., ZHOU, M.: *Dynamic behavior of concrete at high strain-rates and pressures: I. Experimental characterization*, Int. J. Impact Eng., 25:869-886 (2001)
- [6] HAO, Y., HAO, H., LI, Z.X.: *Influence of end friction confinement on impact tests of concrete material at high strain rate*, Int. J. Impact. Eng.; 60:82-106 (2013)
- [7] BISHOFF, P.H., PERRY, S.H.: *Compressive behavior of concrete at high strain rates*, Mat. Struct., 24:425-450 (1991)
- [8] SHARMA, A., OŽBOLT, J.: *Influence of high loading rates on behavior of reinforced concrete beams with different aspect ratios—A numerical study*, Eng. Struct., 79:297-308 (2014)
- [9] HAO, Y., HAO, H., JIANG, G.P., ZHOU, Y.: *Experimental confirmation of some factors influencing dynamic concrete compressive strengths in high-speed impact tests*, Cem. Conc. Res., 52:63-70 (2013)
- [10] CHEN, X., WU, S., ZHOU, J.: *Experimental and modeling study of dynamic mechanical properties of cement paste, mortar and concrete*, Constr. Build. Mater., 47:419-430 (2013)
- [11] OŽBOLT, J., SHARMA, A., REINHARDT, H.W.: *Dynamic fracture of concrete - compact tension specimen*, Int. J. Solids Struct., 48:1534-1543 (2011)

- [12] OŽBOLT, J., LI, Y., KOŽAR, I.: *Microplane model for concrete with relaxed kinematic constraint*, Int. J. Solids Struct., 38:2683-2711 (2001)
- [13] BAŽANT, Z.P., ADLEY, M.D., CAROL, I., JIRASEK, M., AKERS, S.A., ROHANI, B. ET AL.: *Large-strain generalization of microplane model for concrete and application*, J. Eng. Mech. (ASCE), 126(9):971-980 (2000a)
- [14] BAŽANT, Z.P., CANER, F.C., ADLEY, M.D., AKERS, S.A.: *Fracturing rate effect and creep in microplane model for dynamics*, J. Eng. Mech. (ASCE); 126(9):962-970 (2000b)
- [15] DILGER, W.H., KOCH, R., KOWALCZYK, R.: *Ductility of plain and confined concrete under different strain rates*, American Concrete Institute. Special publication. Detroit., USA 1978

